WAKE FLOWS FORCED BY THREE-ELECTRODE PLASMA PULSED ACTUATORS.

Juan D'Adamo, jdadamo@fi.uba.ar
Leandro Leonardo, lleonardo@fi.uba.ar
Federico Castro, fcastro@fi.uba.ar
Roberto Sosa, rsosa@fi.uba.ar
Thomas Duriez, thomas.duriez@gmail.com
Guillermo Artana, gartana@fi.uba.ar
CONICET, FIUBA Universidad de Buenos Aires, Argentina

Abstract. *We study the actuated flow around a cylinder at Re=5500, for which shear layer transition leads to a turbulent wake, with the goal to produce a drag reduction. We considered a three-electrode plasma discharge (TED) actuator and we scrutinized the incidence of two forcing parameters (frequency and amplitude). Particle Image Velocimetry measurements enabled to obtain detailed information and therefore facilitate the comparison of the performance of TED actuator with the canonical dielectric discharge barrier actuator. For the Reynolds number considered, excitation with a TED actuator achieved reductions that attained values as high as 40%. The analysis of vorticity fields complemented with a clustering technique allowed us to gain a physical insight of mechanisms involved particularly when excitation are produced at the resonance frequencies of the wake flow. It comes out from our analysis that spanwise uniform excitation which promote symmetrical vorticity patterns favor drag reductions.*

1. INTRODUCTION

The well-known Bénard-von Kármán (BvK) vortex street results from the destabilization of the steady flow in the wake of the cylinder, driven by the periodic shedding of opposite-signed vortices. The non-dimensional parameter that determines the flow behavior is the Reynolds number, $Re = U_0 D/\nu$, where U_0 is the inflow velocity, D is the cylinder diameter and ν is the kinematic viscosity. Above the threshold $Re_c \approx 47$, BvK dynamics evolve spatially and are associated to an absolute instability that is present over a wide range Reynolds numbers even when the flow becomes three-dimensional for Re$\gtrsim 188$ and turbulence is triggered. Vortex shedding results in vibrations, acoustic noise, enhances the turbulent mixing and contributes significantly to aerodynamic drag in the wake of bluff bodies.

Flow control effectiveness depends on Reynolds number and an extensive review of different techniques can be found in Choi *et al.* (2008). Passive methods included several arrangements like rigid splitter plates, flexible plates or small neighbor cylinder. Among several studies with active devices we can mention: base bleed, blowing-and-suction (Lin *et al.* (1995)); acoustic excitation (Fujisawa *et al.* (2004)); cylinder oscillations that can be rotatory (Thiria & Wesfreid (2007)) or transverse(Blackburn & Henderson (1999)). More recently control by non-uniform spanwise 3D actuators has been studied with passive devices including segmented or wavy trailing edge or active devices like spanwise periodic blowing suctionKim *et al.* (2004).

About 20 years ago, the use of plasma actuators has been proposed as an alternative method to manipulate airflows (see for instance a review by Moreau (2007)). Most of these plasma actuators use non-thermal surface plasmas in which the air flowing close to the surface of the body is weakly ionized. According to Boeuf *et al.* (2007), the presence of charged particles within a highly non-uniform electric field can create a body force near the electrode surface through a collisional mechanism.. Consequently a flow can be superimposed to the ambient air, in still or moving condition, by momentum coupling. Plasma actuators are technologically attractive because of their simplicity, as they have no moving parts, and the very short response time is typically of the order of milliseconds.

A large number of studies with plasma actuators in the last decade have been conducted with dielectric barrier discharges (DBD). The discharge in these devices is produced by applying a high AC voltage between two electrodes that are separated by a dielectric layer. Typically the voltage magnitude is equal to a few kilovolts, the AC frequency range is between 100 Hz and 10 kHz and the dielectric layer thickness ranges from 0.1 mm to a few mm. Under these conditions stable surface plasma can be easily created at atmospheric pressure (Roth *et al.* (2000)).

Different works Artana *et al.* (1999, 2003); MacLaughin *et al.* (2006); Jukes & Choi (2009); D'Adamo *et al.* (2012) among others report results of control the vortex shedding over single cylinders with plasma actuators. Near-wake structure has been studied using time-resolved PIV with simultaneous measurements of the dynamic lift and drag forces. It was shown that the vortex shedding can be suppressed when the velocity of the free stream was relatively low and surface plasma placed near the natural separation point was activated in a pulsed mode at a non- dimensional frequency above $f_f D/U_0 = 0.6$. Some of these works Jukes & Choi (2009) also showed that the lift and drag could be modified for over eight vortex shedding cycles by a short pulse of dielectric-barrier-discharge plasma. Depending on the pulse timing and the plasma location, drag and lift fluctuations could be increased by 7.5% and 87% or reduced by 32% and 70%, respectively.

Also in a recent work, Bhattacharya & Gregory (2015) combined stationary plasma forcing with a spanwise modulation for a cylinder wake at Re=4700. The authors present an important increase of efficiency of the 3D configuration compared to an equivalent 2D actuator that induces similar momentum. While there is a clear difference which favors 3D DBD forcing, 33.6% vs. 3.6% of drag reduction, some open questions arise considering the striking low performance of their stationary 2D DBD when comparing with other results in bibliography as Jukes & Choi (2009); Sosa *et al.* (2009) among others.

The forces produced by a DBD actuator take place in the flow in the proximity of an air-exposed electrode and are localized in a few millimeters. The induced velocities seem to be limited to a few m/s meanwhile ions drift at velocities of the order of 100 m/s. When proposing application of plasma actuators in other environments some scale problems may arise. When applications that involve prototypes of larger size are considered, it is worth using devices that enable to extend the region of actuation to regions of larger size. One of the possibilities is to use series of DBD actuator disposed along the streamwise direction (multistep DBD) as has been proposed by different authors. Other possibility is to use three electrode devices to produce the discharge. Some of these last kind of devices may simultaneously enhance the range of forcing and the region of actuation.

It is therefore of interest to have a better knowledge of the capabilities of these devices in well known benchmarks. In a previous work Sosa *et al.* (2009), we explored the performance of a TED actuators operating in continuous regime mounted on a cylinder. We measured drag forces with a mechanical balance but in this work we lacked of insight on fluid dynamics aspects that accompanied the observed drag reduction.

The present work motivations are based as an extension of our previous study concerning TED forcing on the wake of a cylinder adding the detailed spatial data provided by PIV. Further understanding of flow physics involved is proposed here combining PIV results and clustering techniqueKaiser *et al.* (2014). With this analysis we look forward to bring up new perspective regarding drag and coherent structures behavior.

We organize the paper as follows: in the next section the experimental setup we used in this study is described; in section 3. we show a series of results that characterize TED actuator's induced flow; drag forces estimated from PIV measures are presented on section 4. in section 5. we discuss drag reductions by means of global mode analysis and clustering method; lastly we carry out conclusions in section 6.relating drag measures to forced wake dynamics.

2. EXPERIMENTAL SETUP

The experimental set-up consists of a flow around a circular cylinder at Reynolds number, $Re = 5500$, in the shear layer transition regime. The velocity field measurements were undertaken with a cylinder placed in a closed loop wind tunnel, which has a test section of 50×50 cm^2, where the air velocity is $U_o \simeq 3.30$ m/s. The cylinder has an external diameter $D = 25$ mm, 500 mm long, giving an aspect ratio of 20 and assuring no blockage effects. Given that the Strouhal number $St = f_n D/U \simeq 0.2$, we can estimate roughly the natural vortex shedding frequency $f_n \simeq 26$Hz. Quantitative measurements were performed using 2D Particle Image Velocimetry (PIV) on a vertical plane placed at mid-span of the cylinder. The test section and the whole 130mm $\times$ 90mm imaging region (about 8 $\times$ 6D) divided in interrogation cells of 16 $\times$ 16 pixels gives a spatial resolution of $0.06D$. Sampling frequency was f_S=14.773Hz, a value below f_n so we did not have time-resolved series. We extract the velocity fields from 3 sets of 170 snapshots. The time average velocity fields $\langle \bar{u}(\bar{x}) \rangle$ and velocity fluctuations $\langle {u'_j}^2(x) \rangle$ are determined as:

$$\langle \bar{u}(\bar{x}) \rangle = \frac{1}{N} \sum_{i=1}^{N} \bar{u}(\bar{x}, t_i) \qquad \langle {u'_j}^2(x) \rangle = \frac{1}{N} \left[\sum_{i=1}^{N} (u_j(\bar{x}, t_i) - \langle \bar{u_j} \rangle)^2 \right]^{(1/2)} \tag{1}$$

The incoming free stream flow (U_0) has velocity fluctuation values that are around $2\% U_o$.

Electrohydrodynamic (EHD) actuators are devices that produce a weakly ionized gas and add momentum to the air flow through collisions of charged particles with the neutral species. Among these devices we use a three-electrode discharge (TED) actuator consists of three periodically excited electrodes, which scheme is presented in Fig. 1(a). The electric circuit is composed of a signal generator, an audio amplifier, an ignition coil and a high voltage power source. Electrode A, flush mounted, exposed to the air and electrode B, encapsulated by a dielectric material, conform a typical configuration to produce a DBD actuator. They are separated by the 3 mm thick cylinder wall acting as dielectric barrier. An alternative (V_{AC}) high voltage signal is applied between them. The electrical frequencies and voltages required to produce the DBD are typically in the range of kHz and kV, for our actuator these values were fixed at 9kHz and 11kV at electrode A while electrode B is grounded. Additionally, direct current negative high voltage is applied to electrode A, which tested values where in the range $V_{DC} \in [-6 \ldots -11]$ kV. Beyond 11kV, arc type discharge appears disrupting electrical stability that may damage the equipment.

The electric currents flowing in the system, $I_B(t)$ and $I_C(t)$, were measured with shunt resistances ($R = 50\Omega$).

Figure 1 illustrates how the exposed electrodes are positioned on the surface of the cylinder with their plasma generating edges with respect to the incoming flow direction. Considering the actuators as DBD, $V_{DC} = 0$kV, plasma is formed at $\theta = 80^\circ$ where the angle θ is measured from the stagnation point to the downstream edge of A electrode. This angle is not far from other configurations Jukes & Choi (2009) We wanted to assure a minimal distance between electrodes A

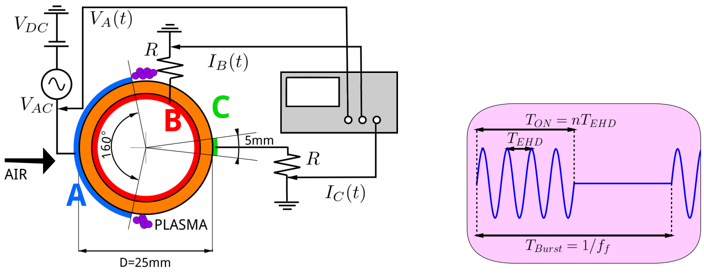

(a) (b)

Figure 1: Schematic and detail of the EHD actuator, electric circuit and input signal with the electrodes flush-mounted.

V_{DC}[kV]	0	6	7	8	9	10	11
P[kW]	559	482	451	429	421	398	425

Table 1: Electrical power consumption for TED actuator.

and C that prevents arc type discharge and allows a wide range of values V_{DC}. However, we must consider that the third electrode is able to extend the plasma formation region.

The signal generator can operate the TED/DBD using a T_{Burst} periodic burst modulation of the sinusoidal high voltage signal as illustrated in Fig. 1(b). The forcing frequency is then $f_f = 1/T_{Burst}$, referred to the natural vortex shedding defines a non-dimensional forcing frequency $f^+ = f_f/f_n$. As we explore values around the natural vortex shedding frequency, $f^+ \in [0.1 \ldots 5]$. On the other hand, the signal duty-cycle, $DC\%$, is defined as: $100 \times (T_{ON}/T_{Burst})$ being T_{ON} the time during which the plasma is produced. This parameter quantifies the fraction of time that the discharge, and consequently the forcing, is active. In this way, by changing this parameter, it is possible to modify the time averaged intensity of actuation.

3. INDUCED ELECTRIC WIND AND POWER CONSUMPTION

In the case of the three-electrode device actuator with $V_{DC} < 0$ the discharge region is extended, taking place between electrodes A and C and it was previously demonstrated, Moreau *et al.* (2008), that the induced momentum increases, respect to that produced by a DBD actuator (i.e.$V_{DC} = 0$), whatever the $x-$position.

In order to quantify the "electric wind" momentum we measured the velocity fields that result from applied TED to the flow around the cylinder at a significantly smaller Reynolds number, Re=400 for $U_0 = 0.24$. Hence, we seed the spatial domain and PIV snapshots could be obtained for a free flow velocity that is considerably smaller than the induced flow. We determine mean flow profiles downstream the cylinder that are shown in Fig. 2(a). We compare velocity profiles $\langle u_x(x = 4)\rangle$ for the non-forced wake flow reference, DBD and TED forced flows. The velocity profiles have a jet flow like shape, that can be characterized by a maximum V_j and a width b. TED results are summarized in Fig. 2(b) where induced momentum is plotted against V_{DC} input voltage. Non dimensional momentum $C_\mu = V_j^2 b/(U_0^2 D)$ compares electric wind induced momentum respect to a characteristic momentum flow in the free stream, $U_0 = 3.3m/s$ corresponding to Re=5500. A strong induced momentum increment is observed from these measures. As DBD actuators produce an asymmetric flow, because the negative DBD discharge, occurring during the negative half cycle, results in a faster velocity than the positive one, Pons *et al.* (2005), TED actuators may profit this behavior. The fluid velocity increases when $V_{DC} < 0$ due to the acceleration of the negative space charge created by the DBD in the negative half-cycle that results higher than the velocity reduction during the DBD positive half-cycle, producing a larger time averaged velocity. On the other hand, Tab. 1 shows the electrical power consumption P[mW/m] for the TED actuator considering several values of V_{DC}. As illustrated in Fig. 1(a), I_B and I_C represents the electric currents collected on B, dielectric barrier electrode and C, the third electrode. While pure DBD configuration, ($V_{DC} = 0$) consumes 565 mW/m, all TED configuration have lower power consumption values with a minimum $P_{min} = 398mW/m$ around $V_{DC} = 10kV$. As we focus on results with $V_{DC} = 11$ kV we retain $P_{TED} = 425$ mW/m as a reference value.

4. CALCULATION OF FORCES WITH PIV

Drag forces have been calculated from velocity fields data. Previous works on this subject have addressed the problem of including the contribution of the pressure field in the momentum balance in a control volume equation:

$$\bar{F} = -\rho \frac{D}{Dt} \int_V \bar{u} dv + \int_S (-p\mathbf{I} + \mathbf{T}) \cdot \bar{n} ds \tag{2}$$

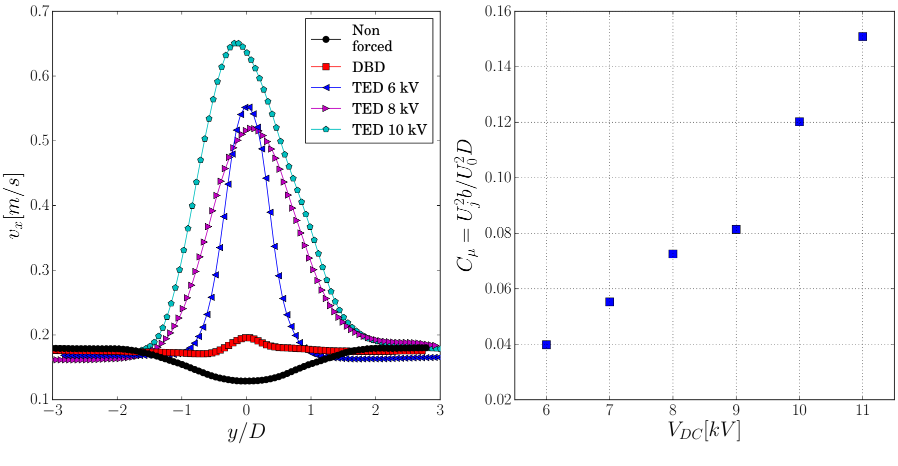

Figure 2: (a) Wake velocity profiles for non-forced and forced flow at $x = 4$. (b) Normalized momentum flux produced by TED actuators.

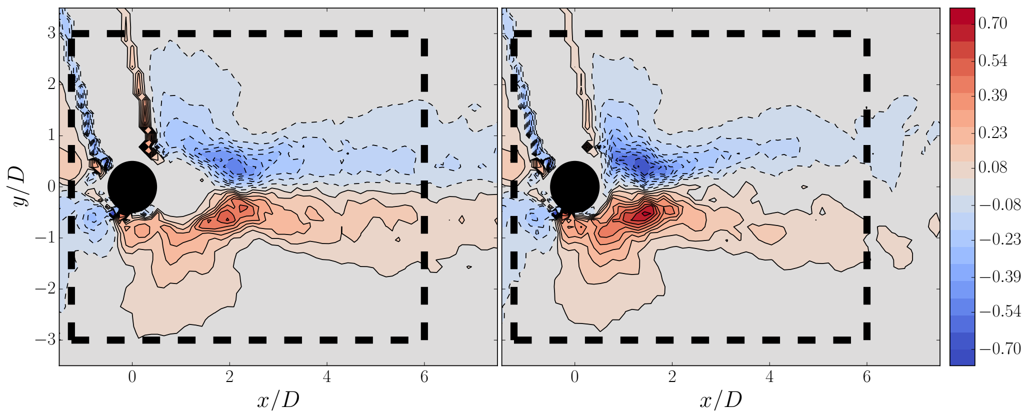

Figure 3: Contour levels for the time averaged $y-$component of pressure gradient $\langle \partial p/\partial y \rangle$ for non-forced flow (a) and under TED V_{DC} =-11kV, $f^+ = 1$ (b). Dashed lines show control volume boundaries.

where V is a control volume, S its boundary, ρ is the fluid density, p is the pressure field, $\mathbf{I}$ the unit tensor and $\mathbf{T} = \mu(\nabla\bar{u} + \nabla^T\bar{u})$ is the viscous stress tensor. The pressure field can be obtained integrating the Navier-Stokes (NS) equation along the control surface Unal *et al.* (1997). Considering for the pressure p along a $s-$curve, $p(s) = p(s-ds) + \nabla p \cdot \vec{ds}$, the latter idea was further refined by Kurtulus *et al.* (2007) who proposed using the NS equation only in the wake region, while adopting the Bernoulli equation in the surrounding slowly-evolving potential flow region. Thus, $p(s) = \partial\phi/\partial t + p_0 - \frac{1}{2}\rho|\bar{u}|^2$ which reduces the numerical error introduced by derivations. Time averaged pressure gradients are hence estimated from PIV data as showed in Fig. 3, where non-forced flow (a) is compared to TED forced case (b), for parameters [$V_{DC} = -11$kV, $C_\mu = 0.15$, $f^+ = 1$]. We observe graphically that besides momentum flux differences from mean flow and velocity fluctuations, pressure fields plays an important role on the determination of the drag force F_D.

Uncertainties were estimated from the RMS value of C_D for a variation of $1D$ on the control volume boundaries that are represented by dashed lines in Fig. 3.

For non-forced flow, $C_D = 2F_x/\rho U_\infty^2 DL \simeq 1.1$ is a value that is in good agreement with available experimental data for Re=5500. Given that changing BvK instability is one of the keys of flow control, it is reasonable to perturb the flow accordingly to the frequencies of natural vortex shedding, following previous control strategies Jukes & Choi (2009). However, stationary forcing was tested for the sake of completeness in the scrutinisation of the control actuator.

First data series compares this value to controlled cases with DBD (electrode C is grounded) and TED enhanced (negative voltage is applied to electrode C) forcing in Fig. 4 characterized by their non dimensional induced momentum C_μ . DBD forcing reduces drag force by about 20% with respect to the non-forced case. Non-pulsed drag measurements by Jukes & Choi (2009) are in the same order of magnitude. Negative voltage is then varied between -6 to 11kv, so C_μ increases according to Fig. 2(b). As a consequence, a monotonic decrease attains a minimum drag value, $C_D \simeq 0.64$ at

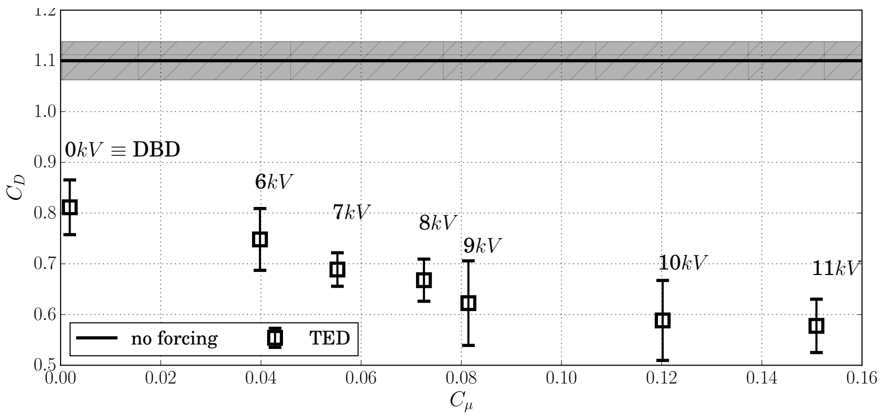

Figure 4: Drag coefficient estimation for non-forced case (solid line), DBD and TED enhanced through stationary forcing mode. Electrode C voltage is decreased from 0 to -11kV so non dimensional momentum C_μ increases monotonically respect to V_{DC}.

$C_\mu = 0.15$, $V_{DC} = -11\text{kV}$, when electrical fields are the highest. In what follows, TED measurements were taken at this value. Next, we performed TED harmonic forcing along with DBD cases for DC=50% and $f^+ \in [0.2\ldots5]$ and the

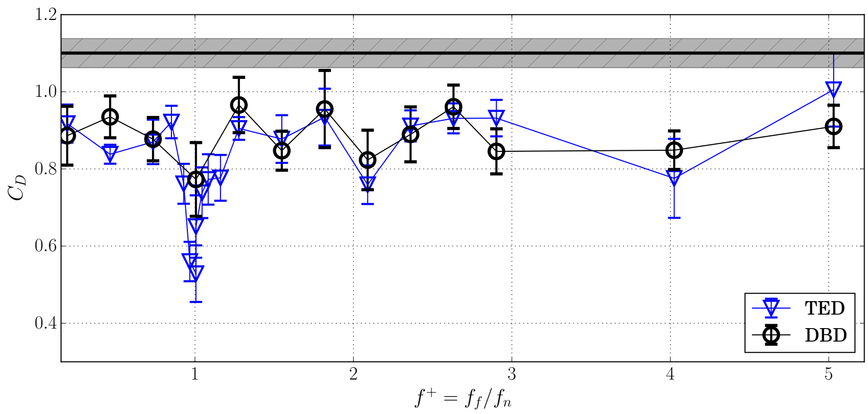

$f^+ = 1$	
DC	C_D
6%	0.98
12%	0.80
19%	0.66
25%	0.67
31%	0.57
37%	0.60
44%	0.57
50%	0.56

Figure 5 & Table 2: Drag coefficient estimation for non-forced case, DBD and TED enhanced (-11kV)) through harmonic forcing at DC=50%. Forcing frequencies $f^+ = f_f/f_0$ are from 0.2 up to 5.0, measurements have been refined around the minimum at $f^+ = 1$. The table shows the how C_D varies at $f^+ = 1$ for duty cycle (DC) values between 6 and 50%.

corresponding drag coefficient results are presented in Fig. 5. Unlike Jukes & Choi (2009) we do not observe a slight increase in drag for DBD forcing frequencies close to the natural vortex shedding frequency; we actually observe for both actuators (DBD and TED) a strong drag reduction near $f^+ = 1$. For this reason, measurements have been refined around this value. The main behavior is similar for both configurations: while drag reductions of about 10 or 20% are obtained for a number of cases, we observe a remarkable decrease on C_D up to 45% for TED at $f^+ = 1$. The first harmonic shows also a small valley for C_D, a 32% reduction, but the main discussion will concentrate on values corresponding to larger reductions at $f^+ = 1$.

Finally, we performed further measurements varying the forcing amplitude through the duty cycle. We were interested on the characterization of the actuator performance around the optimum drag reduction found for TED at $f^+ = 1$. Drag coefficients, estimated for DC values between 6% and 50% are presented in Tab. 2. Major reductions, about 40%, are yet obtained for DC values higher than 30%. Energy saving is possible given this behavior and different control strategies can be undertaken. Drag energy loses for the non-forced flow can be roughly estimated as $P_D = F_D U_0 = \rho C_D U^3 DL/2 =$ 296 mW or $P_D/\text{m} = 592$ mW/m. Recalling power consumption results from Fig. 1, $P = 425$ mW/m for DC=100%, so achieving 40% drag reduction with DC=30% sets up an interesting optimization scenario considering the flow control cost.

Let us remark that we have presented C_D global measurements issued from PIV data so we have access to their corresponding velocity fields in order to discuss and understand the underlying physics of these results.

5. DRAG AND WAKE STRUCTURES

5.1 Mean flow, global modes.

Stationary or harmonic forcings produces mean flow modifications as the principal coherent structures are affected. At Re=5500, even far from the periodic threshold ($Re \simeq 49$) BvK vortex shedding remain the principal structures. We analyze in what follows the components that contributes to the mean drag value in the different cases that have been presented. Non-forced flow field, Figure 6 a), presents the typical counter-rotating vortices for the time-averaged velocity field $\langle \bar{u} \rangle$. A mean recirculation region is usually defined by the contour enclosing of these vortex cells, its principal length is about $\ell_m = 2.5D$. We can compare the flow field with those corresponding to harmonic forcing with DBD (b) and TED (c), where the control parameters duty cycle is fixed to 50% and the forcing frequency $f^+ = 1$ match the largest drag reductions found on Figure 5. We confirm that EHD forcing produces strong modifications in the mean flow fields , as depicted in Fig. 6(b) and (c).where a remarkable decrease of the recirculation region length, about 1 or $1.5D$ is clearly observed.

We can simplify wake flows analysis by considering them as a propagating wave with an amplitude (determined by the fluctuating component of velocity) that grows from the origin, reaches a maximum and decays afterwards. The spatial envelope of this coherent oscillation gives the amplitude of the so-called global mode (see i.e. Wesfreid *et al.* (1996)) , for which the dominant contribution is given by the first harmonics.

The x-distribution, at $y = 0$, of $\langle {u'_y}^2 \rangle$ for non-forced flow and TED harmonic forced cases is presented in Figure 7. The curve for non-forced flow reaches a maximum amplitude $\langle {u'_y}^2 \rangle_M = 0.56$ at $x_M = 2.5D$, which is a measure of vortex formation length(Griffin (1995)). When $f^+ = 0.19$, x_M moves slightly towards the cylinder, and increasing the forcing frequency up to $f^+ = 1$ leads to the closest $x_M \simeq 1.9$. The amplitude of the fluctuations for $\langle {u'_y}^2 \rangle$ is about the same as the non forced case. For greater frequencies, $f^+ = 1.27; 1.54; 2.35$ the amplitude grows up to 0.64. We detailed in Figure 7 inset the behavior of the flow when the forcing frequency is around $f^+ = 1$. Global mode shape changes sensitively when f^+ moves away from 1. We notice that the global mode evolution differs from oscillatory oscillations, see i.e. Thiria & Wesfreid (2007) where the control action is asymmetrical unlike both of our EHD actuators, which induce momentum at the same time from the cylinder walls.

In Jukes & Choi (2009) the authors claim that an intermittent synchronized vortex shedding mode (Figure 17 therein) appears for regimes that matches our forcing parameters. We obtain the same type of vortex pattern inspecting instantaneous vorticity fields of DBD and TED forcing. But we do also observe BvK vortex structures in many snapshots and, since we didn't perform time resolved PIV series, we cannot follow directly the dynamics to affirm whether the flow behaves as reported by Jukes & Choi (2009).

Let us recall that for our reference flow the Strouhal number is $St = fD/U \simeq 0.2$ so the natural vortex shedding frequency is about $f_n \simeq 26$Hz. As we have already mentioned, the acquisition frequency f_S is lower than 15 Hz so we cannot follow the flow dynamics for this velocity. However, when observing periodic motions we have a resource tool that can permit us to elude Shannon-Nyquist limitation: phase averaging acquisition. In this context we should mention that we do not observe a strictly periodic flow because wake turbulence produce small shifts on amplitude and phase of the vortex shedding regime.

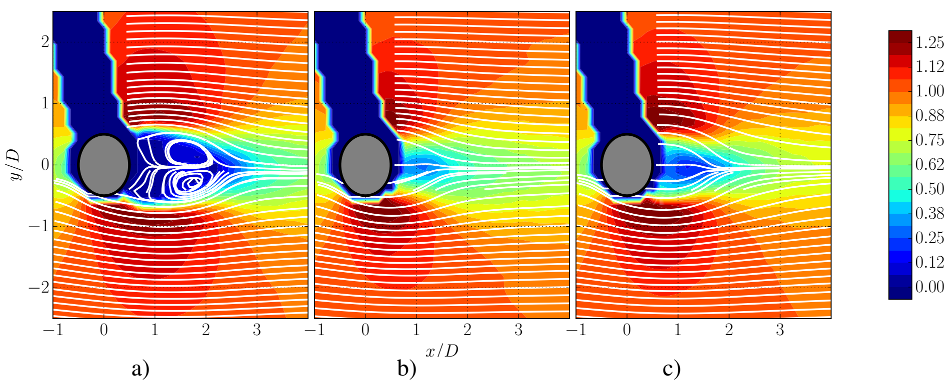

Figure 6: Mean flow streamlines and velocity modulus contours for Re=5500 (a), DBD forcing at $f^+ = 1$(b) and TED forcing at $f^+ = 1$ (c).

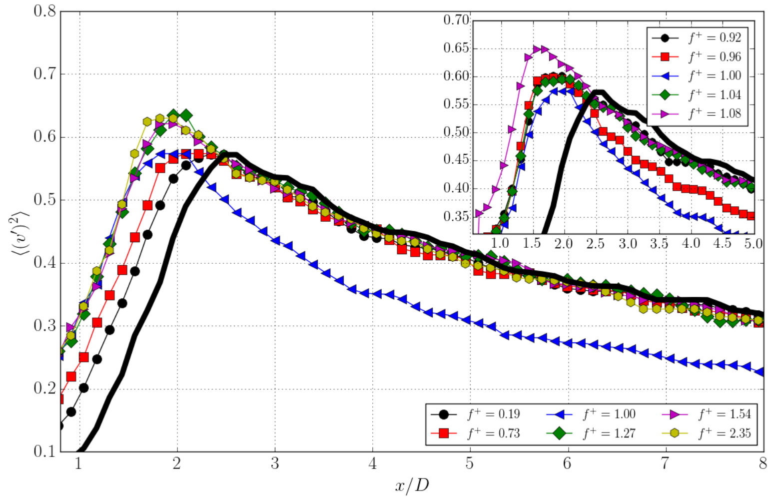

Figure 7: Global mode shape modification under TED actuation for different forcing frequencies. Black thick line stands for global mode of the non-forced case.

5.2 Clustering

For forced flows, periodicity can be established when lock-in regimes are attained. In the present work, even if we perform wake forcing, the induced electric wind velocity is relative small compared to the free flow velocity U so we don't work on lock-in regimes. There is nevertheless one technique that can successfully recover this almost periodically flow dynamics, the clustering technique. Introduced in fluid mechanics framework by Burkardt *et al.* (2006) and later by Kaiser *et al.* (2014), cluster-based method is a promising technique to achieve the analysis of the dynamics for complex flows. Our intention is merely to use the technique in order to retrieve the coherent structures for our wake flow. The method is described in great detail in Kaiser *et al.* (2014) which we summarize in what follows.

We applied the clustering method in order to retrieve the representative states of the wake flow through phase averaging. We use vorticity fields as observations so we can distinguish clearly every phase of the shedding period. Cluster based reduced order modeling relies on the definition of a metric for the determination of similarity between data samples. Considering our space domain Ω in a Cartesian coordinate system where $\mathbf{x} = (x, y, z)$, a number N of vorticity field $\omega(\mathbf{x}, t)$ realizations forms a discrete ensemble $\{\omega^n(\mathbf{x})\}_{n=1}^N$. Vorticity fields are in the Hilbert space $\mathcal{L}^(\Omega)$ of square-integrable vector fields in the domain Ω. An inner product $(f, g)_\Omega$ is defined by $(f, g)_\Omega = \int_\Omega d\mathbf{x} f \cdot g$. In this context we can define the distance between these realizations is the Euclidean distance $D_{mn} = \|\omega^m - \omega^n\|_\Omega$, where the corresponding norm $\|f\|_\Omega^2 := (f, f)_\Omega$. Clustering is a method to order our N realizations or snapshots into into K clusters C_K. Each cluster C_K is represented by its centroid c_k and the standard algorithm, called k-means, consist in three steps: *a)* Initialization of K centroids;*b)* snapshot assignation according to the chosen metric;*c)* Recalculation of each cluster centers as the mean of their corresponding snapshots. The algorithm stops when the clusters converge.

The spatial domain is given by $x \in [1D, 6D]$ and $y \in [-2D, 2D]$ and a number of clusters, 11 according to the total number of snapshots, to describe the flow. Applying the method we recover the phase average vorticity contour levels that are presented in Fig. 8. The number of snapshots that contributes to each cluster is displayed on each frame. The clusters are ordered by means of a cross-correlation algorithm that compares clusters with each other. We obtain in this way a portrait of the main flow dynamics that describes vortex formation and convection over a flow period. BvK structures behavior can be summarized by following the phase dynamics. We obtain cyclic dynamics of the flow, which describe the cylinder flow as a non-linear saturated oscillator limit cycle (Provansal *et al.* (1987)). In order to obtain explicitly a limit cycle description, we made use of proper orthogonal decomposition(POD)Lumley (1967) which is also equivalent to perform a singular value decomposition (SVD) to the data. POD has been used in fluid dynamics extensively and models have evolved significantly (see i.e. Cammilleri *et al.* (2013); Schmid (2010)).

Considering such a decomposition enables us to approximate the vorticity field as the superposition of a a finite set of modes: $\omega(\mathbf{x}, t) = \sum_i a_i(t)\varphi_i(\mathbf{x})$, where a_i and φ_i are respectively called temporal and spatial modes. According to this procedure, snapshots and clusters can be projected on a finite-dimensional subspace generated by a finite number of modes. Fig. 9(a) shows how snapshots and clusters centroids are projected onto the first 3 modes. Each markers (colors) represents ensembles of snapshots belonging to the corresponding cluster. Clusters are numbered from 0, left top frame in Fig. 8 to number 10, right bottom frame. We remark two main characteristics on the vortex arrangement: formation and shedding of vortices are clearly nearer to the cylinder, a BvK-like is depicted from clusters 3 to 10; a novel mode, cluster 0 to 2 presents a symmetrical pattern. Phase-space diagrams in Fig. 9 help to analyze these results. BvK-like mode is

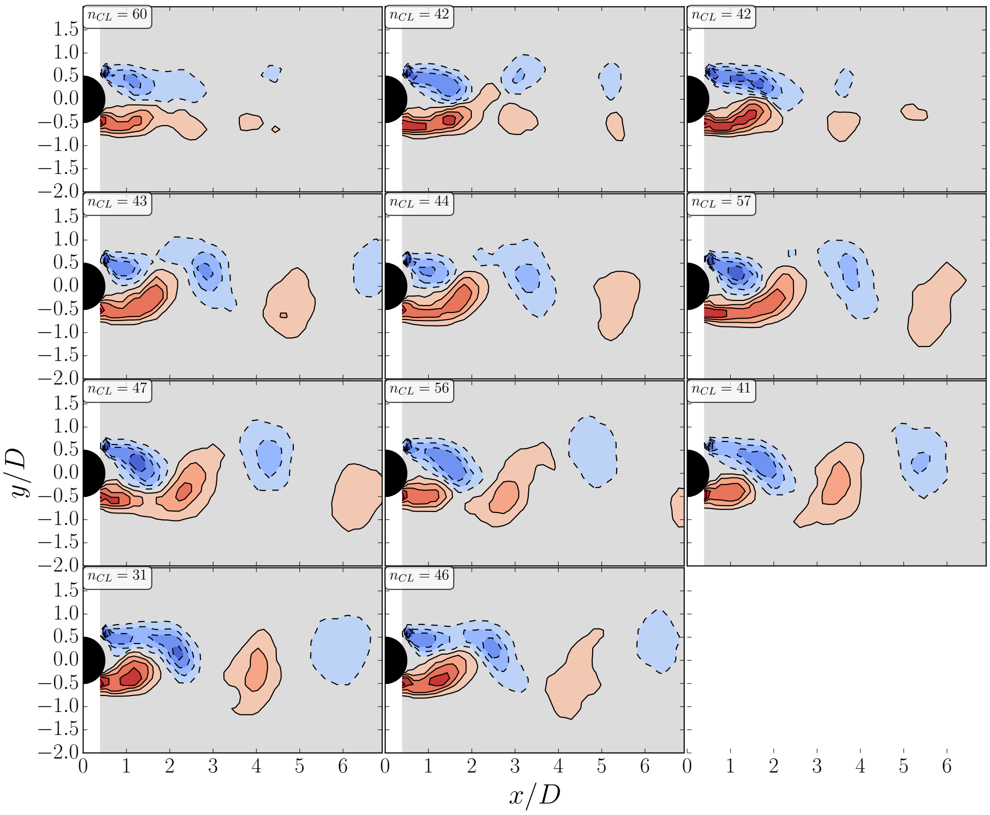

Figure 8: Fourteen clusters portrait the vortex shedding dynamics from vorticity contour lines within one period. The number of snapshots involved are showed in each subplot, initial clusters are placed after the last one to complete a loop. We observe two distinct regimes which corresponds with BvK-like vortex shedding and two vortex sheets produced by TED momentum injection.

distinctly observed in Fig. 9(a) where clusters centroids are coherently connected, following the solid line, from 4 to 10. The symmetric mode, clusters 0 to 3, is centered, equally distant from BvK modes trajectory.

Alternatively, DBD forcing produces similar dynamical states which are represented in phase space of Fig. 9(b). Two trajectories are distinguishable: on one hand BvK-like mode from clusters 1 to 10 and on the other hand cluster 0 stands for symmetric vortex configuration.

There is indeed a higher number of snapshots that belongs to the symmetric mode in TED, 28% of total, than in DBD, %6. TED forcing for our experimental setup favors the formation of this symmetrical mode, which is consistent to the fact that asymmetrical vorticity contribute mainly to drag in wakes as studied by Protas & Wesfreid (2003) from a model proposed by Saffman (1992).

The symmetrical mode may be also associated to the reductions of velocity fluctuations $\langle {u'_y}^2 \rangle$ as observed in Fig. 7. It was reported in the context of studies on propulsive wakes, Raspa *et al.* (2013) that the average of the square of velocity fluctuations is linked to the pressure distribution in the wake. Larger fluctuations produce larger deficits of pressure in the wake and therefore larger drag. The analysis of global modes and clustering enabled us to illustrate how these phenomena are related in forced wakes .

6. SUMMARY AND CONCLUSIONS

We have tested the authority of TED actuators to produce significant drag reductions at Re=5500. Electrical power consumption was measured in order to quantify the cost of the control. The TED at $f^+ = 1$, DC=30% can achieve 40% drag reductions so the power consumed by the actuator is $P_{TED} \simeq 140mW/m$ while the economized power $P_{reduction} \simeq 240mW/m$. The result suggest that the actuator is an efficient tools to govern the flow around bluff bodies and that is robust enough to be considered as a promissory technique for flow control optimization for other Reynolds and geometries. The main interest of our work however does not rely on testing the performance of the actuators but rather on gaining insight of the mechanisms that can explain why the drag reduction is achieved with them.

A first analysis of PIV measurements allowed us to estimate drag forces and to portrait wake fluid dynamics. We

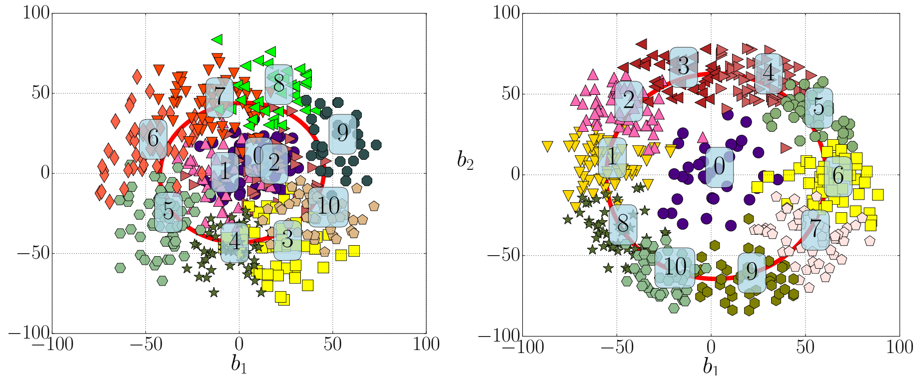

(a) (b)

Figure 9: Phase portrait from SVD of the vorticity clusters, 3 modes are enough to describe the dynamics of vortex shedding modified by actuation. Regimes identified in Fig. 8 correspond to the outer (BvK-like regime) or inner (TED momentum injection) phase space regions.

focused then on harmonic forcing for values in the neighborhood of the natural vortex shedding frequency $f^+ \sim 1$ as at this excitation, significant modifications of the mean flow velocity fields were introduced by TED actuators.

With a global modes analysis we observed that minimum drag is achieved when transverse velocity fluctuations $\langle {u'_y}^2 \rangle$ are smallest at $f^+ = 1$. As proposed by Raspa *et al.* (2013), this result seems to corroborate that when transverse momentum exchange is reduced also occur drag reductions. Unlike rotatory oscillations (in which asymmetry is reinforced by the actuation) we observe that larger reductions take place around $f^+ = 1$.

We used of clustering analysis of vorticity fields. This tool enabled us to educe the dynamics of coherent structures but also allowed us to classify PIV snapshots. Clusters with asymmetric vorticity distributions (in a Bénard Von Kármán vortex like configuration) and clusters in which symmetry of vorticity fields prevails could be identified. In the first kind of clusters, a shortening of the vortex detachment region is visible. The symmetric configuration plays a fundamental role on drag reduction. Some 2D inviscid models may be used to give the theoretical framework that explain why asymmetrical vorticity distributions contribute mainly to drag in wakes.

A complementary analysis can be performed considering the fields of velocity fluctuations. The symmetric configuration has associated lower $\langle {u'_y}^2 \rangle$ that produce more favorable pressure distributions contributing to smaller drag forces.

Thus, a spanwise uniform excitation that promotes larger number of occurrences of symmetric "states" is better suited to reduce drag than forcings that would promote anti-symmetric "states".

7. REFERENCES

ARTANA, G., DESIMONE, G. & TOUCHARD, G. (1999). Study of the changes in the flow around a cylinder caused by electroconvection. *Electrostatics 99 (IOP Publishing Ltd, Bristol–Philadelphia)* , 147–152.

ARTANA, G., SOSA, R., MOREAU, E. & TOUCHARD, G. (2003). Control of the near-wake flow around a circular cylinder with electrohydrodynamic actuators. *Experiments in fluids* **35**(6), 580–588.

BHATTACHARYA, S. & GREGORY, J. W. (2015). Effect of three-dimensional plasma actuation on the wake of a circular cylinder. *AIAA Journal* **53**(4), 958–967.

BLACKBURN, H. & HENDERSON, R. (1999). A study of two-dimensional flow past an oscillating cylinder. *Journal of Fluid Mechanics* **385**, 255–286.

BOEUF, J. P., LAGMICH, Y., UNFER, T., CALLEGARI, T. & PITCHFORD, L. C. (2007). Electrohydrodynamic force in dielectric barrier discharge plasma actuators. j phys d appl phys 40:652. *Journal of Physics D: Applied Physics* **40**(652).

BURKARDT, J., GUNZBURGER, M. & LEE, H. C. (2006). Pod and cvt-based reduced-order modeling of navier-stokes flows. *Comput. Methods Appl. Mech. Eng.* **196**, 337–355.

CAMMILLERI, A., GUÉNIAT, J., F CARLIER, PASTUR, L., MÉMIN, E., LUSSEYRAN, F. & ARTANA, G. (2013). Pod-spectral decomposition for fluid flow analysis and model reduction. *Theoretical and Computational Fluid Dynamics* **27**(6), 787–815.

CHOI, H., JEON, W. P. & KIM, J. (2008). Control of flow over a bluff body. *Annual Review of Fluid Mechanics* **40**(1), 113–139.

D'ADAMO, J., GONZALEZ, L. M., GRONSKIS, A. & ARTANA, G. (2012). The scenario of two-dimensional instabilities of the cylinder wake under ehd forcing: A linear stability analysis,. *Fluid Dynamics Research* **44**, 1–20.

FUJISAWA, N., TAKEDA, G. & IKE, N. (2004). Phase-averaged characteristics of flow around a circular cylinder under acoustic excitation control. *Journal of Fluids and Structures* **19**(2), 159 – 170.

GRIFFIN, O. M. (1995). A note on bluff body vortex formation. *Journal of Fluid Mechanics* **284**, 217–224.

JUKES, T. N. & CHOI, K. S. (2009). Flow control around a circular cylinder using pulsed dielectric barrier discharge surface plasma. *Physics Of Fluids* **21**, 1–12.

KAISER, E., NOACK, B., CORDIER, L., SPOHN, A., SEGOND, M., ABEL, M., DAVILLER, G., OSTH, J., S, K. & K, N. R. (2014). Cluster-based reduced-order modelling of a mixing layer. *Journal of Fluid Mechanics* **754**(9), 365–414.

KIM, J., HAHN, S., KIM, J., LEE, D. K., CHOI, J., JEON, W. P. & CHOI, H. (2004). Active control of turbulent flow over a model vehicle for drag reduction. *Journal of Turbulence* **5**(019), 1–12.

KURTULUS, D., SCARANO, F. & DAVID, L. (2007). Unsteady aerodynamic forces estimation on a square cylinder by tr-piv. *Esp. Fluids* **42**, 187–196.

LIN, J., TOWFIGHI, J. & ROCKWELL, D. (1995). Near-wake of a circular cylinder: control, by steady and unsteady surface injection. *Journal of Fluids and Structures* **9**(6), 659–669.

LUMLEY, J. (1967). The structure of inhomogeneous turbulence. *Atmospheric Turbulence and Radio Wave Propagation* , 166–178.

MACLAUGHIN, T., FELKER, B., AVERY, J. & ENLOE, C. (2006). Further experiments in cylinder wake modification with dielectric barrier discharge forcing. *AIAA Meeting (Reno, USA) paper #2006-1409* .

MOREAU, E. (2007). Airflow control by non thermal plasma actuators. *Journal of Physics D: Applied Physics* **40**, 605–36.

MOREAU, E., SOSA, R. & ARTANA, G. (2008). Electric wind produced by surface plasma actuators: a new dielectric barrier discharge based on a three-electrode geometry. *Journal of Physics D: Applied Physics* **41**(11), 115204.

PONS, J., MOREAU, E. & TOUCHARD, G. (2005). Asymmetric surface dielectric barrier discharge in air at atmospheric pressure: electrical properties and induced airflow characteristics. *Journal of physics D: applied physics* **38**(19), 3635.

PROTAS, B. & WESFREID, J. E. (2003). On the relation between the global modes and the spectra of drag and lift in periodic wake flows. *Comptes Rendus Mecanique* **331**(1), 49–54.

PROVANSAL, M., MATHIS, C. & BOYER, L. (1987). Bénard-von Kármán instability: transient and forced regimes. *Journal of Fluid Mechanics.* **182**(-1), 1–22.

RASPA, V., GODOY-DIANA, R. & THIRIA, B. (2013). Topology-induced effect in biomimetic propulsive wakes. *Journal of Fluid Mechanics* **729**, 377–387.

ROTH, J., SHERMAN, D. & WILKINSON, S. (2000). Electrohydrodynamic flow control with a glow discharge surface plasma. *AIAA Journal* **38**, 1172–1180.

SAFFMAN, P. G. (1992). *Vortex Dynamics*. Cambridge University Press.

SCHMID, P. (2010). Dynamic mode decomposition of numerical and experimental data. *Journal of Fluid Mechanics.* **656**, 5–28.

SOSA, R., D'ADAMO, J. & ARTANA, G. (2009). Circular cylinder drag reduction by three-electrode plasma actuators. *J. Phys.: Conf. Ser.* **166**, 1–14.

THIRIA, B. & WESFREID, J. E. (2007). Stability properties of forced wakes. *Journal of Fluid Mechanics.* **579**, 137–161.

UNAL, M., LIN, J. & ROCKWELL, D. (1997). Force prediction by piv imaging: a momentum-based approach. *J. Fluids Struct.* **11**(8), 965–971.

WESFREID, J., GOUJON-DURAND, S. & ZIELINSKA, B. (1996). Global mode behavior of the streamwise velocity in wakes. *Journal de Physique Paris II* **6**, 1343–1357.